Proceedings of the ASME 2010 International Mechanical Engineering Congress & Exposition
IMECE2010
November 12-18, 2010, Vancouver, British Columbia, Canada

IMECE2010-38682

COMPUTATIONAL MODELING OF LATENT THERMAL ENERGY STORAGE SYSTEM WITH EMBEDDED HEAT PIPES

Karthik Nithyanandam and Ranga Pitchumani*
Advanced Materials and Technologies Laboratory
Department of Mechanical Engineering
Virginia Tech
Blacksburg, Virginia 24061-0238

ABSTRACT:

Due to the intermittent nature of solar energy availability, storing sun's energy in the form of latent thermal energy of a phase change material (PCM) is an effective technique that is widely used in energy storage and load management applications. In a Latent Thermal Energy Storage System (LTES), a heat transfer fluid (HTF) exchanges energy with a PCM. The advantages of an LTES include its isothermal operation and high energy storage density. However, the low thermal conductivity of PCM poses a significant disadvantage due to reduction in the rate at which the PCM can be melted (charging) or solidified (discharging). This paper explores an approach to reducing the thermal resistance of PCM in a LTES through embedded heat pipes. A heat pipe is a passive heat transfer device that efficiently transfers large amount of energy between the PCM and HTF thus indirectly amplifying the effective thermal conductivity of PCM. A transient computational analysis of a shell and tube LTES embedded with heat pipes is performed for charging to determine the position of melt front and energy stored as a function of time. The influence of the number and orientation of heat pipes and design configuration of the system is analyzed to identify configurations that lead to improved effectiveness.

INTRODUCTION:

Fossil fueled power plants are detrimental to the environment and efforts are underway to replace fossil fuels with renewable energy sources including solar energy. Concentrated solar power plants (CSP) capture the solar energy and store as heat which can be used to drive a turbine and produce electricity. CSP thus provide low-cost energy generation and have the potential to become the leading source of renewable energy for future power generation. But, due to the intermittent nature of solar energy availability, it is often desirable to store energy for use on demand including times when solar energy is unavailable. Energy can be stored either as sensible heat or latent heat of which latent heat storage is more advantageous due to its high volumetric energy density and high Rankine cycle efficiency owing to their isothermal operation.

In the LTES system, HTF exchanges energy with a PCM. The operation of LTES constitutes two cycles namely, charging and discharging. During charging, hot HTF obtained by the concentration of solar energy onto it exchanges energy with the PCM resulting in the melting of PCM. During the discharging cycle, PCM transfers heat to the circulating cold HTF resulting in the solidification of the PCM. The hot fluid obtained may then be used to produce steam in order to run the turbine and generate electricity. Usually, the charging cycle occurs during the day when solar energy is available while the discharging cycle aids in producing electricity even when the solar energy is not available.

A fundamental challenge with LTES is the low thermal conductivity of the PCM which significantly reduces the rate of heat transfer between the PCM and HTF. To alleviate this, use of heat pipes which can efficiently transfer heat from one end to the other by means of evaporative cooling thus increasing the heat transfer rate between the HTF and PCM is explained in the present work. The thermal working cycle of a heat pipe involves the evaporation of working fluid at the high temperature end creating a high vapor pressure. Due to the pressure difference, the vapor migrates along cavity to the low temperature end where it condenses back to fluid and absorbed by the porous wick. The condensed working fluid flows back to high temperature end by means of capillary action. Since the return mechanism is not gravity assisted as in thermosyphons, the orientation of heat pipes is immaterial. Heat pipes are capable of transferring large amounts of energy nearly isothermally, can be custom-tailored in performance by carefully selecting the working fluid and its operating pressure as well as the wall material, and can be fabricated in a wide variety of shapes.

Numerous researches analyzing the melting/solidification of PCM in LTES have been found in the literature. Ng et al. [1] investigated the melting of PCM stored in a cylindrical annulus using finite element method. The results showed recirculation cells representative of the natural convection within the PCM which were modeled by the Boussinesq approximation. Horbaniuc et al. [2] modeled the solidification of a low-melting temperature PCM surrounding a longitudinally finned heat pipes. By simulating a two-dimensional solidification of the PCM they demonstrated that the usage of more fins lead to increased solidification rates. Trp [3] investigated numerically a two-dimensional model of a shell and tube LTES configuration and quantified the thermal performance by analyzing the

* Corresponding author. +1 540 231 1776; pitchu@vt.edu

temperature distributions within the PCM. Guo et al. [4] analyzed numerically the performance of LTES system equipped with KNO_3-$NaNO_3$. The enhancement in performance when the PCM is interspersed with aluminum foils is quantified by analyzing the time history of the liquid fraction within the PCM. Khodadadi et al. [5] simulated two-dimensional melting and solidification of a PCM mixed with copper nanoparticles. The natural convection effects were included by means of the Boussinesq term. Farid et al. [6] presented a brief review on the materials used as PCM for LTES. Jegadheeswaran et al. [7] summarized a comprehensive review on the researches carried out in LTES field over the past decade. The major contributions include the analysis of the performance enhancement in LTES embedded with fins or interspersed with metal particles. Tardy et al. [8] investigated numerically and experimentally use of heat pipes to melt a low-melting temperature PCM.

Several papers ranging from in model complexity of heat pipes are found in the literature. Zuo et al. [9] presented a simple network model of heat pipe and the results compared favorably with the profiles obtained from the two-dimensional model developed by Cao et al. [10] for a sodium-stainless-steel heat pipe. In the simple network model developed, the effect of vapor core on the operation of heat pipes was considered negligible. The network model is based on the heat conduction within the wall and the wick. Sobhan et al. [11] simulated a two-dimensional model of flat heat pipes accounting for all the mechanisms occurring within. The transient operation of heat pipes was clearly depicted. Kaya et al. [12] presented a detailed three-dimensional model of heat pipe and analyzed its transient operation.

Apart from the studies on the analysis of LTES and heat pipes separately, a comprehensive study on the enhancement in the performance of a LTES embedded with heat pipes in PCM is not carried out. The objective of the present study is, therefore, to analyze the improvement in the performance of two different configurations of LTES by embedding heat pipes. A brief parametric analysis is also carried out to obtain the optimum orientation of heat pipes and design configuration of the system which increased the melting rate of PCM and the performance enhancement was quantified by measure of the effectiveness of the LTES system.

MATHEMATICAL MODEL

A tube-in-shell configuration is considered for the present study. Figure 1(a) illustrates a unit cell for the configuration of HTF considered to pass through the tubes embedded within the PCM which is referred to as Module 1. In another configuration, PCM is stored in a tube and the HTF flows over it as illustrated for a unit cell in Fig. 1(b) which will be referred to as Module 2. Figures 1(a) and 1(b) define the computational domain for the present study and the unit cell in both the cases have a periodically repeating nature forming a complete LTES system. Figure 1(c) shows a schematic of the longitudinal cross-section of the embedded heat pipes along with the symbols denoting the various pertinent dimensions for the modeling.

The flow of the heat transfer fluid is considered incompressible. The properties of PCM are considered to be constant in both the solid and the liquid phases. The change in the HTF temperature from the inlet to outlet of either module is

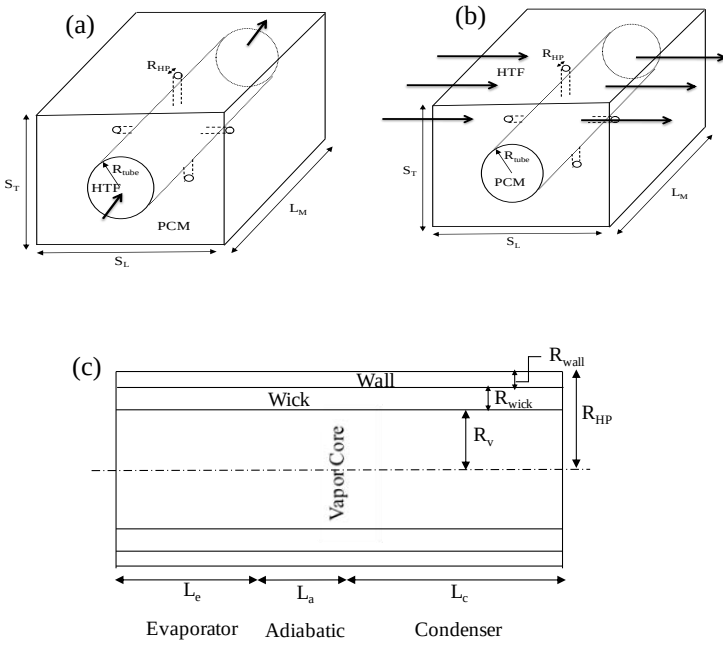

FIGURE 1 Schematic of LTES (a) Module 1 (b) Module 2 (c) Heat Pipe cross section

considered negligible. The natural convection effects are modeled by the Boussinesq approximation.

The melting-solidification process within a PCM is modeled by the enthalpy-porosity technique as illustrated by Voller et al. [13]. By this approach, the porosity in each cell is set equal to the liquid fraction in the cell. Based on the melted region, for each iteration, the liquid fraction, γ takes either the value of 1 for a fully liquid region, or 0 for a solid region, or $0< \gamma <1$ for a partially solidified region (mushy zone). Accordingly, the coupled system of continuity, momentum and energy equations governing the processes in both HTF and PCM are as follows:

$$\nabla.(\rho\vec{V}) = 0 \tag{1}$$

$$\nabla.(\rho\vec{V}\vec{V}) = -\nabla p + \nabla.\vec{\tau} + S \tag{2}$$

$$\nabla.(\rho c_p \vec{V} T) = \nabla.(k^{eff}\nabla T) \quad \text{(HTF and Walls)} \tag{3a}$$

$$\frac{\partial}{\partial t}(\rho H) + \nabla.(\rho\vec{V}H) = \nabla.(k\nabla T) \quad \text{(PCM)} \tag{3b}$$

where $S = \rho\vec{g}$ for HTF and $S = \rho\vec{g}\beta(T - T_{ref}) - A(\gamma)\vec{V}$ for PCM; ρ is the phase density; $\vec{V}$ the superficial velocity vector with components u in the *x*-direction, *v* in the *y*-direction and *w* in the *z*-direction ; $\vec{\tau}$ the stress tensor; $\vec{g}$ the gravity vector which is 0 ms^{-2} in the horizontal direction and 9.8 ms^{-2} in the vertical direction; *T* is the temperature and T_{ref} is chosen to be the melting point temperature of PCM. The source term for PCM includes the Boussinesq approximation term as the first

term and the porosity function, $A(\gamma) = \frac{C(1-\gamma)^2}{\gamma^3 + \varepsilon}$ as the second term which makes it to mimic the Carman-Kozeny equation for flow in a porous media, where, ε = 0.001 is a small computational constant to avoid division by zero and C is a constant reflecting the morphology of the melting front set at 1.6×10^6 as defined by Brent et al. [14]. In the energy equation, Eqs. 3(a) and 3(b) , total enthalpy, H can be expressed as $H = h + \Delta H$ where h represents the sensible heat defined as $h = h_{ref} + \int_{T_{ref}}^{T} c_p dT$ and $\Delta H = \gamma h_{sl}$ represents the latent enthalpy. c_p stands for the specific heat of PCM at constant pressure and h_{sl} is the latent heat of PCM.

The modeling of heat pipe follows the simplified equivalent thermal resistance network model developed by Zuo et al. [9], which accounts for the conduction within the wick and the heat pipe wall and neglects the effect of evaporation-condensation within the vapor core and advection of the working liquid within the capillary. The mathematical details of the network model are omitted here for brevity but may be found in Zuo et al. [9] and are not repeated here. The thermal resistance network model of [9] was implemented in the present work based on its computational simplicity without loss of accuracy as reported in [9]. In the present implementation, the effective wick thermal conductivity was calculated as $k_{eff} = \frac{k_l[(k_l + k_s) - (1-p)(k_l - k_s)]}{[(k_l + k_s) + (1-p)(k_l - k_s)]}$ while the effective heat capacity was expressed as $(\rho c)_{eff} = (1-p)(\rho c)_s + p(\rho c)_l$ where p is the porosity of the wick, the subscripts s and l represent the solid phase of the wick namely, stainless steel and liquid phase of the wick, sodium, respectively.

The complete model of the system described above was implemented in a commercial finite-volume based computational fluid dynamics solver, FLUENT using the geometrical and physical parameters listed in Tables 1 and 2. The temperature within the PCM was solved for by iterations involving the energy equation, Eq. 3(b) and liquid fraction relation as suggested by Voller et al. [13]. The dimensions of the LTES presented in Table 1 are representative of those used for large scale energy storage [15]. Sodium-Stainless steel heat pipe is used for the present analysis [16] while the HTF and PCM material are KNO_3 and Therminol respectively [15]. The thermal network modeling of heat pipes as presented in ref. [9] was implemented in FLUENT through a user defined function. The computational grid was built of hexahedral elements with an optimal interval spacing after careful examination of the results of the grid refinement process. The SIMPLE algorithm has been used for the pressure-velocity coupling and the time step in the calculation was set at 0.1 s and further decrease to 0.05 s did not show any noticeable changes in the instantaneous results for the melt fraction throughout the whole process, ranging from t = 0 to t = 12 hours which is taken as the average length of a day. The convergence was checked at each time step with the residual convergence criteria of 10^{-5} for momentum and continuity equations and 10^{-8} for energy equation.

TABLE 1: Geometrical parameters used in the computational modeling [15]

Heat Pipe	
Outer radius, R_{HP} [m]	0.018
Condenser section length, L_c [m]	0.14
Evaporator section length, L_e [m]	0.1
Adiabatic section length, L_a [m]	0.06
Wall thickness, w_{HP} [m]	0.001
Wick porosity, p	0.9
Effective wick thermal conductivity, k_{eff} [W/m-K]	45
Effective wick heat capacity, $\rho c_{peff,}$ [J/m^3-K]	1.05×10^6
Tube	
Module Length, L_M, [m]	0.12
Wall thickness, w_t [m]	0.003
Outer radius, R_t [m]	0.5

TABLE 2: Physical parameters of HTF , PCM and wall used in computational modeling [15]

	PCM KNO_3	*HTF* *Therminol*	*Stainless Steel*
Density, ρ [kg/m^3]	2109	709	7900
Thermal Conductivity, k [W/m-K]	0.5	0.078	20.1
Specific heat, c_p [J/kg-K]	953	2588	559.9
Dynamic Viscosity, μ [Pa-s]	2.59×10^{-3}	0.152×10^{-3}	-
Melting point, T_m [K]	664	-	-
Thermal expansion coefficient, β [K^{-1}]	200×10^{-6}	-	-
Latent heat of fusion, h_{sl} [J/kg]	95×10^3	-	-

Apart from the geometrical and physical parameters listed in Tables 1 and 2, respectively, the other input parameters include the inlet mass flow rate and inlet temperature of HTF which were set at 2.89 kg/s and 664 K for Module 1 and 0.917 kg/s and 664 K for Module 2, respectively, which correspond to a total flow rate resulting in the generation of 80MW$_e$ solar power using Therminol. The inlet and outlet flow were implemented as periodic conditions for both Module 1 and Module 2 with the rest of the planes in the geometry implemented as symmetry boundary condition due to its repeating nature. The tube wall and the heat pipe wall adjoining both PCM and HTF were solved as coupled boundary conditions. From the numerical simulations, the contours of the melt front at different instants of time, and the instantaneous energy stored within the PCM obtained as output were used to explore the performance of the two different configurations of the LTES for different orientation of heat pipes and the results are presented in the following section.

RESULTS AND DISCUSSION

The following section presents results obtained from the numerical simulation with heat pipes either mounted horizontally or vertically for both Module 1 and Module 2 are presented in this section. The simulations were performed for the charging process for a maximum period of 12 hours which is assumed to be the average length of a day for which hot HTF are available.

Figures 2(a)–(d) present the contours of the volume fraction of the PCM at various instants of time during the charging process for Module 1. Figure 2(a) represents the initial contour of the volume fraction where the PCM is in the solid state with the initial temperature being its melting point temperature. Figure 2(b) portrays the same at a time instant of 4.16 h, where it can be seen that the melting of the PCM is symmetric about one quadrant of the tube. No convection cells were observed and the melting of PCM up until this point is purely conduction dominated. From Fig. 2(c), it can be seen that the melting of PCM is no longer symmetric. This is due to the free convection flow that occurs as a result of the temperature difference between the heated wall and relatively cold solid phase. Thus, the lighter melt at the bottom of the tube rises along the wall to the top, being heated in the process and when it returns upon cooling, it exchanges heat with the adjoining solid phase thus entraining more fluid and forming a clockwise vortex. This ensures relatively faster melting of the PCM at the top of the tube compared to the bottom. From Fig. 2(d), it is seen that more molten PCM from the top is liquidified implying amplification in the strength of the convection currents. It is also noted that the whole domain is symmetric about the vertical diametral axis only and accordingly, the rest of the simulations for Module 1 were carried out for one half of the domain.

Figures 3(a)–(d) show the simulated phase distribution of the melting of PCM embedded with 2 horizontal heat pipes at 0 h, 4.16 h, 6.94 h, 12 h from the start of the process. The contour at the inset depicts the melt front in the vicinity of heat pipes as seen from the top. From Fig. 3(a), it can be observed that the melt fraction contour in the vicinity of heat pipes clearly delineates the adiabatic section from the condenser section of the heat pipe. Figure 3(b), which represents the volume fraction contours at a time instant of 4.16 hours shows that the melting is still conduction dominated. But due to the horizontal heat pipe, convection cells are formed along it's condenser section and a recirculation zone was observed in the horizontal direction. As time progressed, convection cells were also formed in the vicinity of the tube which is observed in Fig. 3(c). Unlike in the previous case, hot fluid from the bottom rises along the heated wall to the top and while returning circulates along the melt front formed around the heat pipe thus resulting in an increased melting of PCM. The same phenomena is observed in Fig. 3(d), as the two recirculation free convection cells around the heat pipe and tube merged into one strong zone. The liquid volume fraction that has been melted in this case at 12 hours is 25.1% which is 1.46 times greater than compared to that of the module without any heat pipes.

Figures 4(a)–(d) represent the liquid fraction contour plots of the molten PCM embedded with two vertical heat pipes at various instants of time. As in the previous cases, convection cells around the tube are formed only after a time period of 4

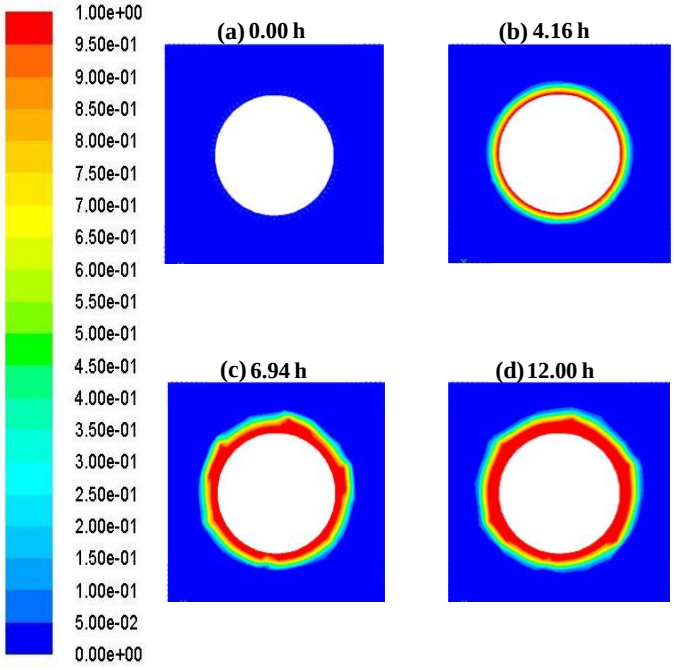

FIGURE 2: Colorized contours of the volume fraction of the PCM at various time instants for Module 1

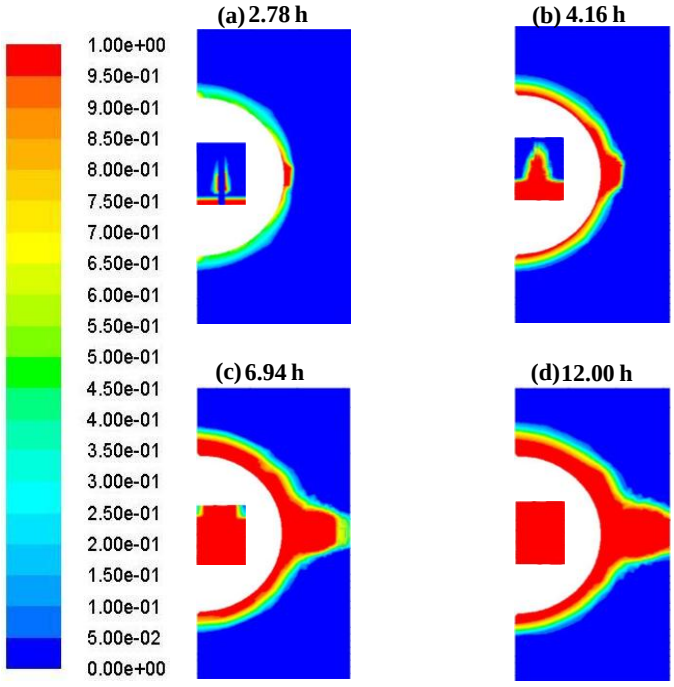

FIGURE 3: Colorized contours of the volume fraction of the PCM at various time instants for Module 1 embedded with 2 horizontal heat pipes.

hours. The melting is purely conduction dominated up until 4.16 hours as observed in Figs. 4(a) and 4(b) except for the free convection that takes place around the heat pipes. As time progressed, the melt front in the vicinity of the top vertical heat pipe grows faster due to the natural convection which brings in hot melt from the bottom to the top due to the buoyant force. It is also noticed that the vertical heat pipes have a slower impact on the melting of the PCM for the same.

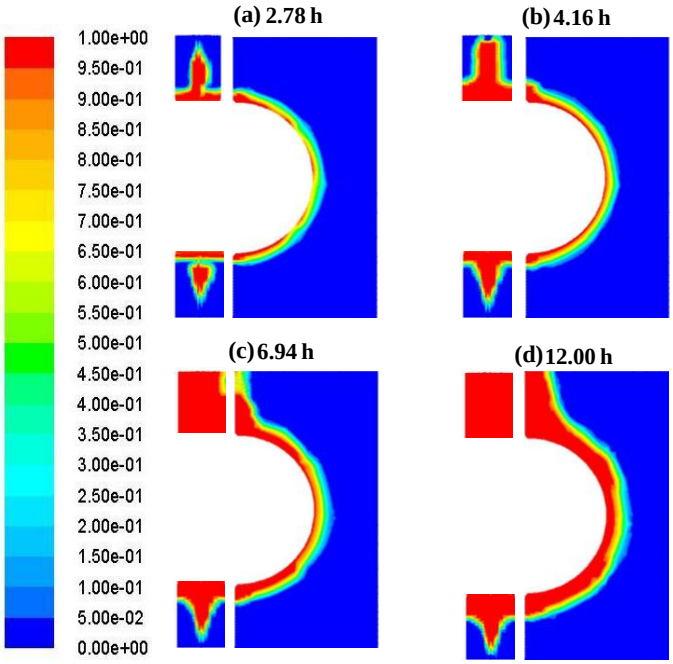

FIGURE 4: Colorized contours of the volume fraction of the PCM at various time instants for Module 1 embedded with 2 vertical heat pipes.

Since the natural convection effect results in a slower charging at the bottom part of the PCM, installing a heat pipe at the bottom does not contribute much to the enhancement in the melting rate of the PCM. From Fig. 4(d), it can be observed that at the final instant of time, the top portion of the PCM adjacent to the heat pipes is completely melted while the PCM at the bottom has not. The total fraction of the volume of the molten PCM in this case at the final instant of time was found to be 21.1% which is slightly less compared to the case with two horizontal heat pipes. On further analysis, it was found that though the heat transfer between the vertical heat pipes and HTF is higher compared to the horizontal heat pipes, the natural convection phenomena enhances the melting process further in the case of Module 1 embedded with horizontal heat pipes.

Figure 5 portrays the liquid fraction at various instants of time for Module 2. To ensure a fair comparison, the inlet mass flow rate for this case was kept at 0.917 kg/s ensuring that the mass flow rate per unit volume of the PCM is kept constant for both the configurations. Figure 5(a) shows the initial volume fraction of the PCM as totally solid. Figure 5(b) which portrays the contours of the volume fraction at 4.12 hours shows that not sufficient liquid is formed to start a natural convection process and the melting of PCM up until this instant is conduction dominated. The convection cells formed in this case have been found to be stronger and this could be attributed to the lesser surface area and height of the PCM region. Hence, though Module 2 seems to have a higher fraction of the PCM volume melted compared to Module 1, the melting rate of PCM is only slightly higher as discussed later. The total fraction of the PCM that has been melted at the end of the process is found to be 50.4%.

Figures 6(a)–(d) represent the liquid fraction contour plots of the molten PCM embedded with two vertical heat pipes.

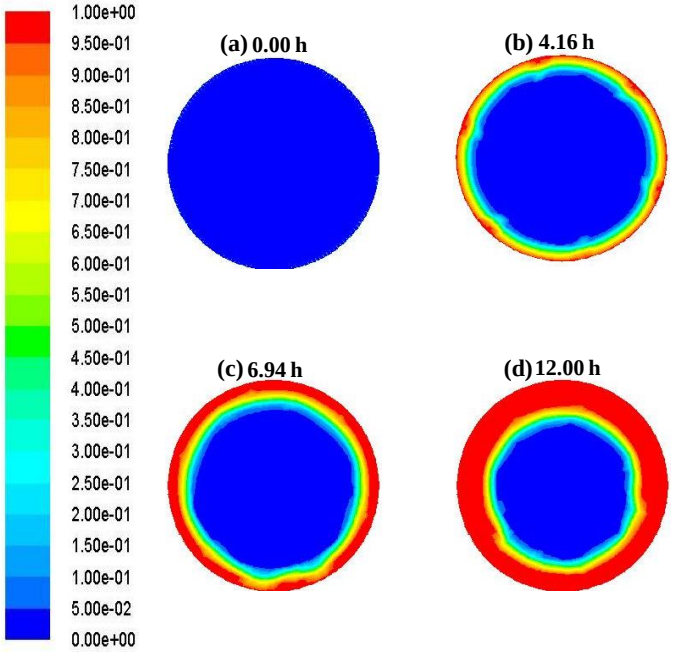

FIGURE 5: Colorized contours of the volume fraction of the PCM at various time instants for Module 2.

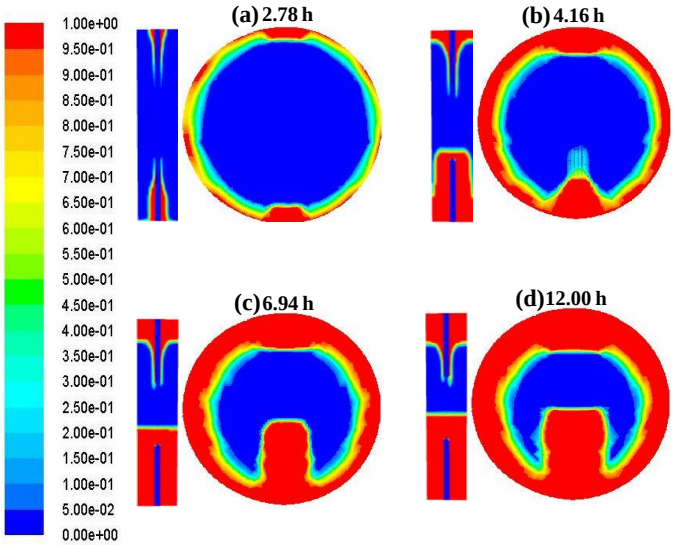

FIGURE 6: Colorized contours of the volume fraction of the PCM at various time instants for Module 2 embedded with 2 vertical heat pipes.

Figure 6(a) portrays the conduction dominated melting of the PCM. At a time instant of 4.16 hours, the contours of volume fraction as seen in Fig. 6(b), shows that the convection cells are formed which is sooner compared to the previous cases. It was observed that the melt front in the vicinity of the heat pipes has not begun to grow due to the slower heat transfer rate between HTF and HP when compared to Module 1. As time progresses the stronger convection cells are formed circulating hot fluid from the bottom along the walls of the tube to the top. But comparing Figs. 6(c). and 6(d), it is observed that the melt front at the bottom part of the PCM seems to grow faster. This is due to the fact that thermal stratification is

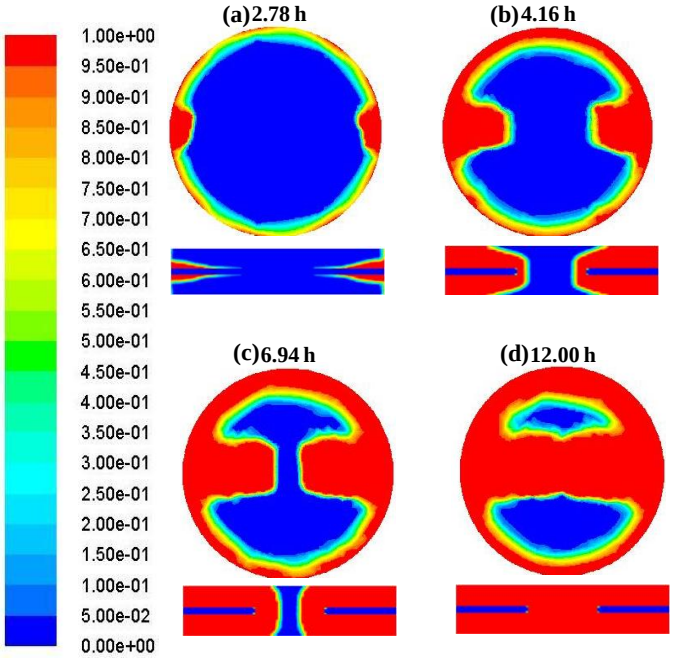

FIGURE 7: Colorized contours of the volume fraction of the PCM at various time instants for Module 2 embedded with 2 horizontal heat pipes.

observed in the upper part of the PCM with the top region being hot compared to the bottom region and the circulation zone extends from the bottom to the middle of the PCM only.

Figures 7(a)–(d) represent the liquid fraction contour plots of the molten PCM embedded with two horizontal heat pipes. As observed for Module 1 in Fig. 4., convection cells were found to be formed along the horizontal heat pipe also. As observed in Figs.7(b)–(d), in due course of time, the convection cells along the tube and heat pipe coalesce into one zone resulting in an efficient melting in the upper part of the PCM while the PCM at the bottom part of the tube remains in the solid state. Thus energy is used to raise the temperature of the PCM which is mainly carried upward by the convective flow in the melt. The vortex formed in the convection cell were found to circulate from the bottom along the tube to just below the top of the tube and moves along the melt front surrounding the axis of the heat pipe before returning to the bottom. The fraction of the volume that has been melted in this case at the end of the process was found to be 71.8% which is 1.42 times greater than that of Module 2 without any heat pipes.

Figure 8(a) depicts the time history of the energy stored within the PCM for the three cases simulated for Module 1. It is observed that the rate of melting is the highest for LTES system embedded with two horizontal heat pipes. To quantify the augmentation in the performance of LTES system due to the usage of heat pipes a quantity called the Effectiveness is defined as, $\varepsilon = \frac{Q_{t,HP}}{Q_t}$, where $Q_{t,HP}$ is the energy stored for the case of tube embedded with heat pipes while Q_t represents the energy stored for the case without any heat pipes. From Fig. 8(b), it can be seen that there is a sharp increase in the effectiveness curve at a time of approximately 4.2 hours for both horizontal and vertical heat pipes. This can be attributed to the start of the convection dominated melting in Module 1 as opposed to the conduction dominated melting which prevailed until then. After that instant of time, the effectiveness remains fairly constant for both the cases. It is also observed that installing horizontal heat pipes provide greater augmentation in performance compared to vertical heat pipes and the effectiveness was found to be 1.46 at the end of 12 hours.

Similarly, Figs. 9(a) and 9(b) show the time history of energy storage and effectiveness respectively for Module 2. It is observed that though the fraction of the volume that has been melted in the case of Module 2 is far greater than that of Module 1 the latent energy stored in Module 2 over a period of 12 hours is slightly lesser than Module 1 implying lesser melt volume. Also, the effectiveness of the heat pipes follow the same pattern as observed in Fig. 8. The augmentation of thermal performance by the usage of horizontal heat pipes is observed to be more when compared to vertical heat pipes. The effectiveness value for LTES embedded with horizontal heat pipes was 1.42 at the end of the charging cycle. The findings of the present study detailed the enhancement in the melting rate of PCM embedded with two horizontal and two vertical heat pipes for two different configurations of LTES. Future studies will involve a more detailed modeling of heat pipes to analyze its impact on the performance of LTES for both charging and discharging cycles and also explore other number and orientation of heat pipes such as three heat pipes with an angular spacing of 120^o and four heat pipes oriented at 90^o to each other.

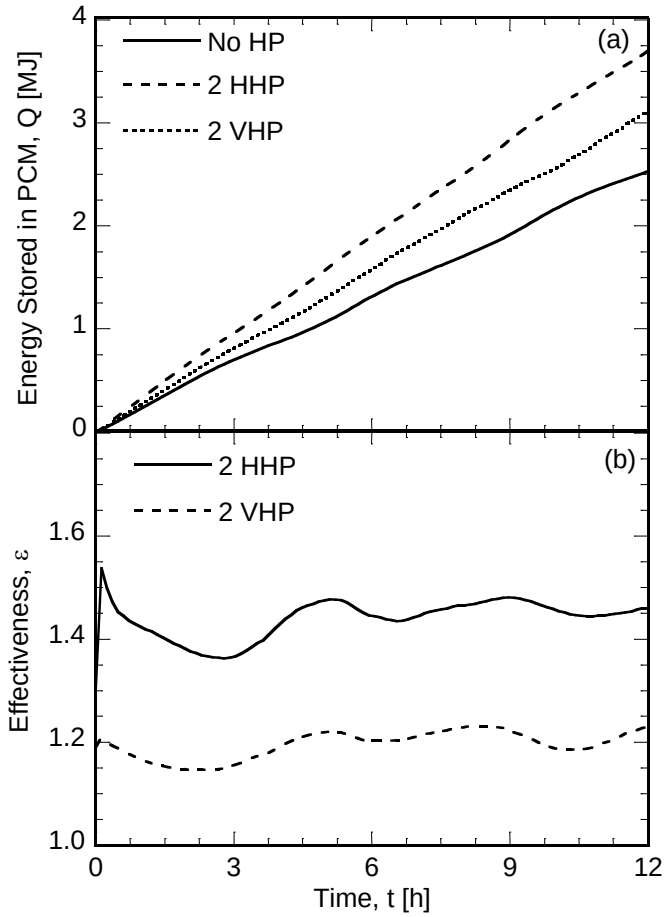

FIGURE 8: Effect of the orientation of heat pipes on the (a) Energy stored and (b) Effectiveness for Module 1

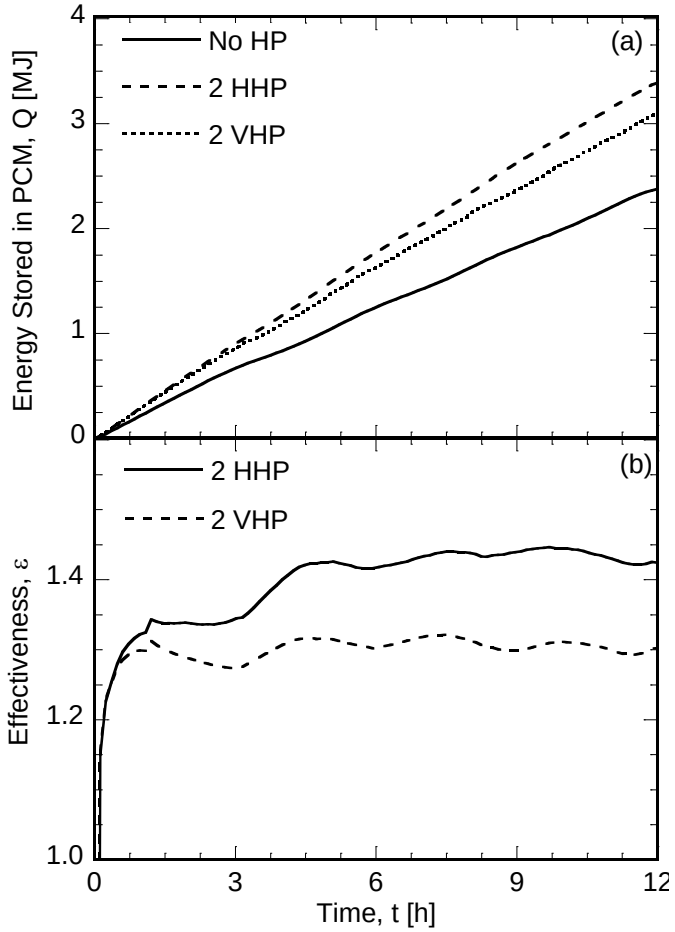

FIGURE 9: Effect of the orientation of heat pipes on the a) Energy stored and (b) Effectiveness for Module 2

CONCLUSIONS

The results presented in this paper illustrate a methodology to determine the performance enhancement in LTES due to the usage of heat pipes. It was found that higher effectiveness was attained for the case of horizontal heat pipes for both the configurations considered. Module 2 resulted in higher melt fraction compared to Module 1 while the energy stored in the case of Module 1 was higher. The results also showed that the natural convection currents mainly influenced the performance of heat pipes as opposed to the heat transfer between HTF and heat pipes while thermal stratification was clearly observed in Module 2. Overall, Module 1 embedded with horizontal heat pipes provided the best thermal enhancement.

ACKNOWLEDGMENTS

This work was supported by a grant from the U.S. Department of Energy under Award Number DE-FG36-08GO18146. Their support is gratefully acknowledged.

NOMENCLATURE

c_p specific heat [J/kg-K]
h sensible enthalpy [J/kg]
H total enthalpy [J/kg]
HHP Horizontal Heat Pipes
k thermal conductivity [W/m-K]
h_{sl} latent heat [J/kg]
L length [m]
p porosity
Q latent energy stored [J]
R radius [m]
T temperature [K]
u x-component velocity [m/s]
v *y*-component velocity [m/s]
VHP Vertical Heat Pipes
w *z*-component velocity [m/s]

Greek symbols:

β thermal expansion coeffeicient [K^{-1}]
ϵ effectiveness
φ wick porosity
ρ density [kg/m^3]
μ dynamic viscosity [Pa-s]
γ liquid fraction

Subscripts:

a adiabatic
c condenser
e evaporator
HP heat pipes
t HTF tube
t,HP HTF tube with heat pipes

REFERENCES

[1] Ng, K.W., Gong, Z.X., Mujumdar, A.S., 1998, "Heat Transfer in Free Convection-Dominated Melting of a Phase Change Material in Horizontal Annulus," *Int. Comm. Heat Mass Transfer*, 25(5), pp. 631–640.

[2] Horbaniuc, B., Dumitrascu, C., Popescu, A., 1999, "Mathematical model for the study of solidification within a longitudinally finned heat pipe latent heat thermal storage system," *Energy Conversion Mgmt.*, 40, pp. 1765-1774.

[3] Trp, A., 2005, "An Experimental and Numerical Investigation of Heat Transfer During Technical Grade paraffin Melting and Solidification in a Shell-and-Tube Latent Thermal Energy Storage Unit," *Solar Energy*, 79, pp. 648–660.

[4] Guo, C., Zhang, W., 2008, "Numerical Simulation and parametric Study on New Type of High Temperature Latent Heat Thermal Energy Storage System," *Energy Convers. Mgmt.*, 49, pp. 919-927.

[5] Khodadadi, J.M, Hosseinizadeh, S.F., 2007, "Nanoparticle-Enhanced Phase Change Materials with Great Potential for Improved Thermal Energy Storage," *Int. Comm. Heat and Mass Transfer*, 34, pp. 534-543.

[6] Farid, M.M., Khudhair, A.M., Razack, A.A.K., Al-Hallaj, S., 2004, "A Review on Phase Change Energy Storage: Materials and Applications," *Energy Conv. and Mgmt."*, 45, pp. 1597–1615.

[7] Jegadheeswaran, S., Pohekar, S.D., 2009, "Performance Enhancement in latent Heat Thermal Storage System: A Review," *Renew. Sustainable Energy Reviews*, 13(9), pp. 2225-2244. [8] Sobhan, C.B., Garimella, S.V., Unnikrishnan, V.V., 2000, "A Computational Model for the Transient Analysis of Flat Heat Pipes," *Inter. Societ Conference on Thermal Phenomena*, pp. 106–113.

[8] Tardy, S., Sami, S.M., 2009, "Thermal Analysis of Heat Pipes During Thermal Storage," *Appl. Therm. Eng.*, pp. 329-333.

[9] Zuo, Z.J, Faghri, A., 1998, “A network thermodynamic analysis of the heat pipe,” *Int. J. Heat and Mass Transfer*, 41, pp. 1473–1484.
[10] Cao, Y., Faghri, A., 1990, "A Transient Two-Dimensional Compressible Analysis for High Temperature Heat Pipes with Pulsed Heat Input," *Numerical heat Transfer*, 18, pp. 586-594.
[11] Sobhan, C.B., Garimella, S.V., Unnikrishnan, V.V., 2000, "A computational model for the transient analysis of flat heat pipes," *Int. Soc. Conference on Thermal Phenomena*, pp. 106-113.
[12] Kaya, T., Glodak, J., 2007, "Three Dimensional Numerical Analysis of Heat and mass Transfer in Heat pipes," *Heat Mass Transfer*, 43, pp. 775-785.
[13] Brent, A.D., Voller, V.R., Reid, K.J., 1988, "Enthalpy-Porosity Technique for Modeling Convection-Diffusion Phase Change: Application to the Melting of a Pure Metal," *Numer. heat Transfer*, 13, pp. 297-318.
[14] Voller, V.R., Cross, M., Markatos, N.C., 1987, "An Enthalpy Method for Convection/Diffusion Phase Change," *Int. J. Numer. Methods*, 24, pp. 271–284.
[15] Shabgard, H., Bergman, L., Sharifi, N., Faghri, A., 2010, "High Temperature Latent Heat Thermal Energy Storage using Heat Pipes,” *Int. J. Heat and Mass Transfer*, 53, pp. 2979-2988.
[16] Faghri, A., 1995, “Heat Pipe Science and Technology,” *Taylor and Francis*.